Self-Reinforcing Elastomer Composites Based on Ethylene–Propylene–Diene Monomer Rubber and Liquid-Crystalline Polymer

S. Chakraborty, N. G. Sahoo, G. K. Jana, C. K. Das

Materials Science Centre, Indian Institute of Technology, Kharagpur 721302, India

Received 3 September 2003; accepted 23 January 2004
DOI 10.1002/app.20482
Published online in Wiley InterScience (www.interscience.wiley.com).

ABSTRACT: In this study, the prime factor determining the size, shape, and distribution of liquid-crystalline polymer (LCP) was the viscosity ratio at the processing conditions. The fiber-forming capacity of the LCP depended on the viscosity of the ethylene–propylene–diene monomer rubber (EPDM). With increasing LCP content, the tensile and tear strengths did not increase, perhaps because of incompatibility between the EPDM and LCP. The hardness increased because of the hard mesogenic groups in the LCP. The percentage swelling decreased as the LCP content increased. With increasing LCP content, processability became easier because of a lower melt viscosity. The scorch time increased at higher LCP levels. A higher percentage crystallinity was observed with increasing LCP content. Scanning electron microscopy clearly showed the fiber phase formation, which was two-dimensionally isotropic in nature, confirming fiber formation even in a shear field. The addition of LCP improved the thermal stability. The onset degradation temperatures shifted to higher values with increasing LCP content. Dynamic mechanical thermal analysis revealed that with the addition of LCP, the mechanical damping increased at its lower level. High-temperature processing increased the effective amorphous zone. © 2004 Wiley Periodicals, Inc. J Appl Polym Sci 93: 711–718, 2004

Key words: liquid-crystalline polymers (LCP); incompatibility; X-ray; thermogravimetric analysis (TGA); mechanical properties

INTRODUCTION

The most important parameter governing the fibrillation of liquid-crystalline polymer (LCP) in blend is the viscosity ratio and the strain rate.[1–4] In the case of flexible-chain polymer blends, the deformation and breakup of the dispersed phase is governed by the viscosity ratio and the Weber number.[5–11] It has been reported that the effect of fibrillation is enhanced as the viscosity ratio of LCP to matrix thermoplastics becomes less than 1.[12–15] However, the available information is very sketchy concerning the effect of the Weber number on the fibrillation. It has also been reported that the elongational flow causes more extensive fibrillation than the shear flow.[16–19] With increasing extension ratio, the LCP phase is transformed from spherical to globular and then to a fibrillar form. Previous literature[20–22] has indicated that LCP augments the crystallization process of the semicrystalline thermoplastic phase and, thus, improves the composite properties. A very exhaustive study was done with LCP–thermoplastics blends,[23–28] but very limited information is available with regard to the LCP–elastomers blends. Seo and coworkers[29–30] dealt with ethylene–propylene–diene monomer rubber (EPDM)/LCP blends and suggested the effect of elongational deformation on the microfibrils of LCP. Sahoo and Das studied the self-reinforcing characteristics of LCP in ethylene–propylene–rubber (EPR).[31] Verhoogt et al.[32] studied blends of Kraton and LCP, suggested that the polymers were immiscible, and observed a shift in the glass-transition temperature (T_g) due to the adsorption of the elastometric phase on LCP particles.

With the effect of viscosity on the fibrillation of LCP taken into consideration, this study was undertaken with EPDM (ethylene/propylene ≈ 75/25) and a thermotropic LCP. Static and dynamic properties and failure mechanisms were correlated with the phase morphology and the crystallinity of the composites.

EXPERIMENTAL

The EPDM used was Royalene 539 (Uniroyal Co., USA), and the LCP used was Vectra A950 (Hoechst-Celanese, USA). The LCP had a comonomer composition of 73% hydroxybenzoic acid and 27% hydroxynaphthonic acid. The curative used was dicumyl peroxide (Verox-40KE, R. T. Vanderbilt Co., Inc., USA). The mixing formulation is shown in Table I. The mixture of LCP with EPDM was done with a Brabender plasticorder (PL-2200, N50E mixer; Germany)

Correspondence to: C. K. Das (ckd@matsc.iitkgp.ernet.in).

TABLE I
Compounding Formulations

Ingredient	L_0	L_1	L_2	L_3	L_4
EPDM	100	90	80	70	60
LCP	0	10	20	30	40
Verox-40KE (phr wrt EPDM)	1.85	1.85	1.85	1.85	1.85

TABLE II
Physical Properties

Physical property	L_0	L_1	L_2	L_3	L_4
100% modulus (kgf/cm^2)	7.8	11.0	11.3	10.0	—
200% modulus (kgf/cm^2)	18.3	21.2	24.0	20.0	—
Tensile strength (kgf/cm^2)	49.2	36.0	33.0	22.5	19.0
Elongation at break (%)	935	745	435	230	100
Tear strength (kgf/cm)	20.0	13.2	8.0	6.5	5.5
Hardness (shore A)	72	74	77	79	80

at 300°C for 6 min. The blended compound was then mixed with dicumyl peroxide at 100°C in the Brabender plasticorder for 4 min. The mixed compound was then sheeted out from the two-roll mixing mill and vulcanized by compression molding up to 30 min at 150°C and at 20 MPa. All of the properties were determined from the vulcanized slabs thus prepared. The slab dimensions were 15 × 15 × 0.15 cm. The cure characteristics of the blends were studied in a Monsanto rheometer (R-100; USA) at 150°C. The tensile properties of the blends were tested on a universal tensile testing machine (KMI, India) at a test speed of 50 cm/min. Swelling was carried out in tetrahydrofuran (THF) at room temperature for 48 h.

An X-ray diffraction (XRD) study was done with the help of a PW-1840 X-ray diffractometer (Phillips PW 1710, Holland) with a cobalt target (Co Kα) at a scanning rate of 0.05° 2θ/s, a chart speed of 10 mm/2θ, a range of 5000 c/s, and a slit of 0.2 mm, with 40 kV and 20 mA applied to assess the change in the crystallinity of the blends as affected by the blend ratio.

The area under the X-ray diffractrogram was determined in arbitrary units. The degree of crystallinity (X_c) and the amorphous content (X_a) were measured with the following relationships:

$$X_c = I_c/(I_a + I_c) \times 100, \quad X_a = I_a/(I_a + I_c) \times 100$$

where I_c and I_a are the integrated intensities corresponding to the crystalline region and the amorphous halo, respectively, as described earlier.[33,34] Peak halfwidth (β), crystallite size (P), and interplanar distance (d) were calculated as follows:[33,34]

$$\beta = \text{Area of peak/Height of peak} \times 1/5$$

$$P = 92.35/\beta \cos \theta$$

$$d = 1.793/2 \sin \theta$$

Differential thermal analysis (DTA)/thermogravimetric analysis (TGA) studies were carried out with a Shimadzu DT-40 instrument (Tokyo, Japan) in the presence of air at a heating rate of 20°C/min within the temperature range 20–1000°C.

A VA-4000 viscoanalyzer (Metravib RDS, France) was used to measure the dynamic parameters, including storage modulus, loss modulus, stiffness. and tan δ, within the temperature range 20–300°C. The stiffness values were taken from the original plots and plotted as a function of blend ratio.

The dynamic fracture mechanisms of the blends were studied by scanning electron microscopy (SEM; JSM-5800, Jeol, Japan), the surface was auto-sputter-coated with gold at a 0° felt angle.

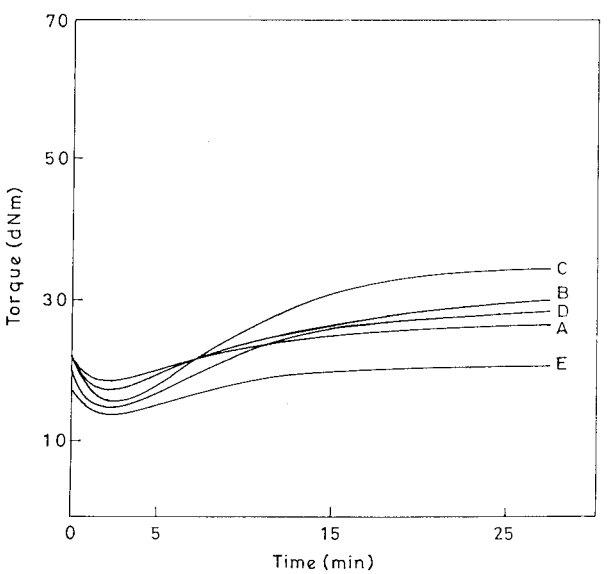

Figure 1 Variation in the rheometric torque with cure time: (a) L_0 (100% EPDM), (b) L_1 (90/10 EPDM/LCP), (c) L_2 (80/20 EPDM/LCP), (d) L_3 (70/30 EPDM/LCP), and (e) L_4 (60/40 EPDM/LCP). The slab was made at 150°C.

TABLE III
Percentage Swelling of Samples-Made at 150°C with Curative

Sample	Swelling (%)
L_0	43
L_1	41
L_2	40
L_3	39
L_4	37

TABLE IV
Percentage Swelling of Samples Made at 300°C Without Curative

Sample	Swelling (%)
L_0	Highly swelled mass
L_1	64
L_2	58
L_3	55
L_4	51

TABLE V
XRD Parameters of Samples Made at 150°C with Curative

Sample	Crystallinity (%)	2θ (°)	d (A°)	P (A°)
L_0	24	23.7	4.35	15.7
L_1	29	23.9	4.32	17.4
L_2	32	24.3	4.25	19.4
L_4	34	24.6	4.19	22.6

RESULTS AND DISCUSSION

Processing and mechanical properties

The cure characteristics of pure EPDM and the blends were studied at 150°C and are shown in Figure 1; the corresponding physical properties are given in Table II. As shown in Figure 1, minimum torque (t_{min}), that is, the melt viscosity, decreased with increasing LCP in the blend. This was due to the rigid rod-like LCP molecules, which helped the molecular planes to slip past each other by acting as an internal lubricant. The state of cure [maximum torque (t_{max}) − (t_{min})] increased up to 20% of the level of LCP and then decreased with the addition of more LCP in the blend. The scorch time initially decreased (sample L_1) and then increased with LCP content in the blend. The tensile strength value decreased with the addition of LCP in the blend. This was due to the lower interfacial adhesion between the LCP and the EPDM phase, which acted as weak point to generate cracks, and thus, failure occurred at a lower applied load. The modulus values of these blends increased up to a concentration of 20% LCP and then decreased. However, the modulus of these blends was always higher than the modulus of EPDM because of the presence of rigid mesogenic groups in LCP. The tear strength decreased with the addition of LCP, which was in line with tensile strength. The elongation at break of these blends decreased with the addition of LCP because of the increase in the blend stiffness. The hardness, however, showed the reverse trend. A low tensile strength with low elongation at break suggested a lack of strain-induced crystallization as the LCP content was increased. LCP can impart crystallinity, and these crystal domains were very stiff and less compressible, which made the blend harder.

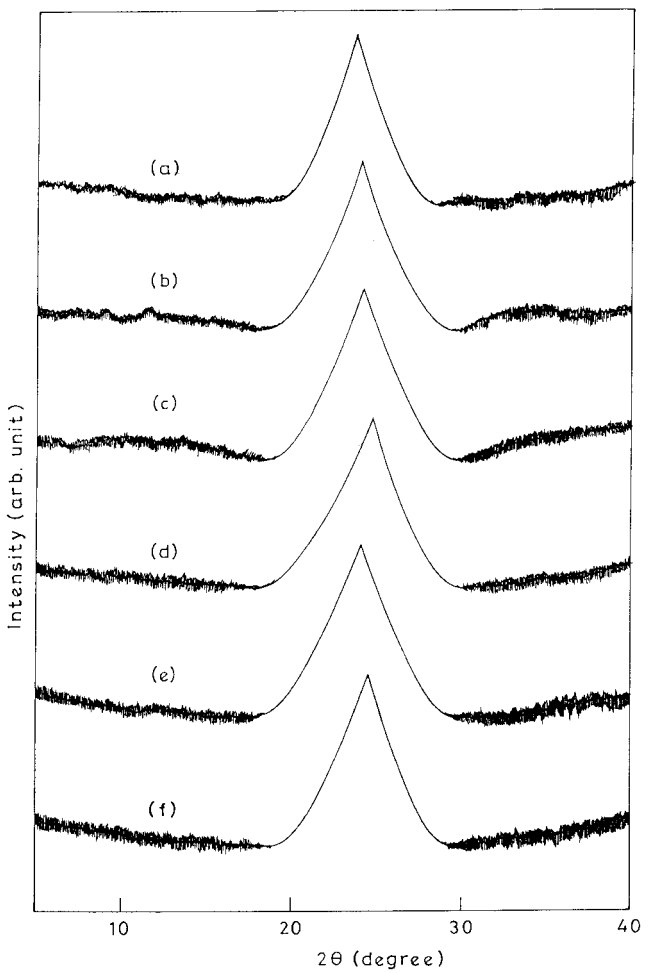

Figure 2 X-ray diffractograms of (a) L_0 (100% EPDM, 150°C), (b) L_1 (90/10 EPDM/LCP, 150°C), (c) L_2 (80/20 EPDM/LCP, 150°C), (d) L_4 (60/40 EPDM/LCP, 150°C), (e) L_2 (80/20 EPDM/LCP, 300°C, without curative), and (f) L_4 (60/40 EPDM/LCP, 300°C, without curative).

Swelling study

The percentage swelling of each sample was studied in THF, and the results are given in Tables III and IV. For cured samples (with curative, Table III), the maximum swelling was observed for pure EPDM. The percentage swelling decreased with increasing LCP because of the increased crystallinity of the blends. Because of similar reasons, the percentage swelling

TABLE VI
XRD Parameters of Samples Made at 300°C Without Curative

Sample	Crystallinity (%)	2θ (°)	d (A°)	P (A°)
L_2	30	24.0	4.30	20.6
L_4	33	24.3	4.25	24.6

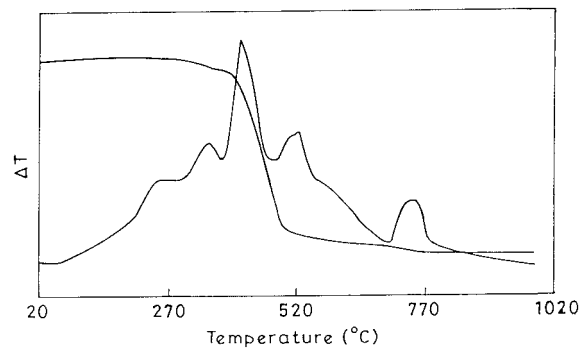

Figure 3 DTA/TGA plot of the L_1 sample cured at 150°C.

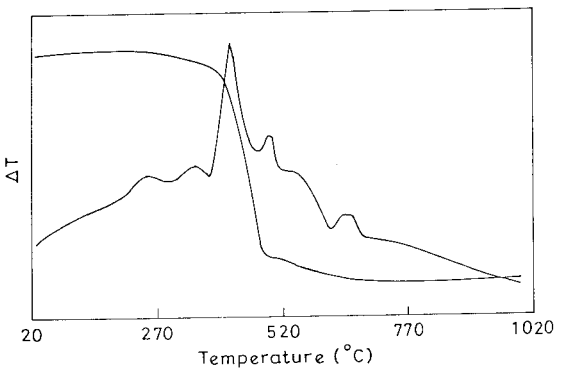

Figure 5 DTA/TGA plot of sample L_1. The slab was made at 300°C without curative.

decreased with increasing LCP content for the slabs made at 300°C (Table IV) without curative. In this case, there was no crosslinking, as we did not add any crosslinking agent. So, the amount of swelling in each case was higher than that of the samples made with curative (Table III). This phenomenon corroborated the reinforcing character of LCP, probably because of its fibrillation characteristics.

X-ray study

X-ray diffractograms of the various blends are shown in Figure 2, and the respective parameters are given in Tables V and VI. Crystallinity is affected by the blend composition and crystallization conditions, such as temperature, pressure, orientation, molecular weight, and diluents.[35] As shown in Tables V and VII, the percentage crystallinity increased with increasing LCP content in the blend. At high LCP content, the increase in crystallinity was associated with increasing P, suggesting favored growth of the crystal domain. However, there was slight decrease in the crystallinity of the samples made at 300°C without curative (Table VI) compared to those made in the presence of curative. With increasing LCP in the blend with EPDM, d decreased marginally, suggesting compactness in the blend system structure. High-temperature (300°C) processing gave rise to a slightly lower crystallinity, associated with an increased P. This phenomenon suggested a predominant effect of the cooling rate toward the formation of crystal domains with a favored growth mechanism, which resulted in more effective amorphous zones.

Thermal analysis

The DTA/TGA plots are shown in Figures 3–6, and the thermal parameters are shown in Tables VII and VIII. As shown by TGA, the degradation mainly occurred in two steps. The pure EPDM exhibited its first degradation temperature (T_1) around 235°C. The addition of LCP to EPDM resulted an increasing degradation temperature, with the blend containing 40% LCP exhibiting a degradation temperature as high as 337°C. So, T_1 shifted toward the higher temperature side with increasing LCP content. The second degradation of EPDM was started at 498°C. At a lower level of LCP (10%), the second degradation shifted to a higher temperature side (505°C). However, for the blend at a higher level of LCP (40%), the second degradation started at a higher temperature (548°C) than EPDM and L_1. The percentage weight loss (in the first

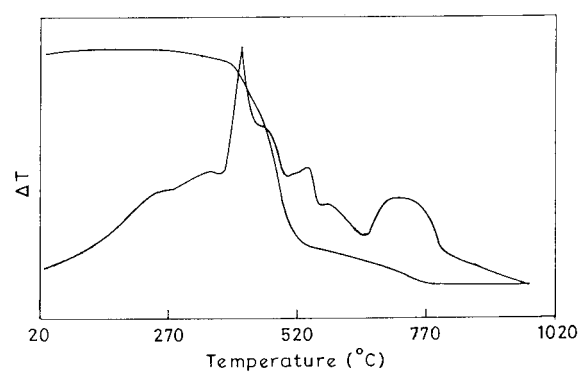

Figure 4 DTA/TGA plot of the L_4 sample cured at 150°C.

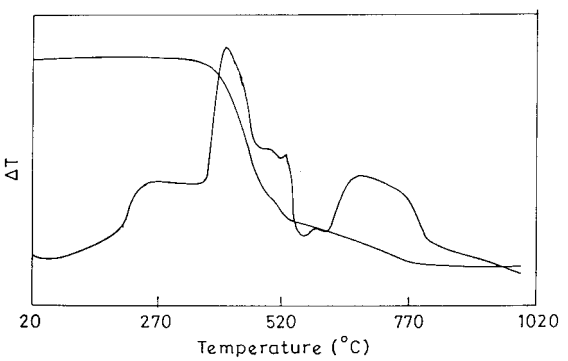

Figure 6 DTA/TGA plot of sample L_4. The slab was made at 300°C without curative.

TABLE VII
DTA/TGA Parameters of Samples Made at 150°C with Curative

Sample	T_1 (°C)	T_2 (°C)	Weight loss (%) for the first step	T_{50} (°C)
L_0	235	498	86	387
L_1	315	505	80	434
L_4	337	548	72	490

T_2 = second degradation onset temperature.

step) decreased with increasing LCP content in the blend. From the previously discussed trend of change, it was evident that the LCP-rich blend was thermally more stable than the pure EPDM sample. The 50% decomposition temperature (T_{50}) increased with increasing LCP in the blend, thus lowering the rate of oxidative decomposition. It is well known that the oxidation of a polymer occurs in the amorphous region because the crystallites are impermeable to oxygen.[36] Crystallinity enhanced the thermal stability of the LCP-rich blends. This conclusion was also supported by the results of the sample taken from the slab made at 300°C without curative. In this case, the T_1 and the completed temperature values were relatively lower than the corresponding values of the cured samples (made at 150°C). Because of crosslinking and crystallinity, the thermal stability of the cured samples were improved compared to the samples made at 300°C without curative. As shown in Figures 3–6, a broad exothermic peak in the DTA thermograms was observed, which was due to oxidative degradation of the EPDM rubber. TGA plots showed that the maximum weight loss occurred in this region. Because the oxidative degradation process was a complex one, the degradation of the uncrosslinked phase, degradation of the low-level crosslinked phase, volatile matter formation, degradation of unused curative, and so on also occurred and, hence, produced more peaks at later stages.

Dynamic mechanical thermal analysis

The variation of tan δ with temperature is shown in Figure 7. The relaxation spectra for the blends (L_1 and L_2) showed three distinct loss peaks. However, for pure EPDM, only one broad loss peak, around 134°C, was evident. This relaxation spectrum of EPDM shifted to the lower temperature side at 130°C for L_1 and 126°C for L_2 with increasing LCP content in the blend. The loss peak around 216°C (for blend L_1) also shifted to the lower temperature side, that is, 180°C (for blend L_2). These two high-temperature relaxation

TABLE VIII
DTA/TGA Parameters of Samples Made at 300°C Without Curative

Sample	T_1 (°C)	T_2 (°C)	Weight loss (%) for the first step	T_{50} (°C)
L_1	302	505	81	427
L_4	302	540	62	482

T_2 = second degradation onset temperature.

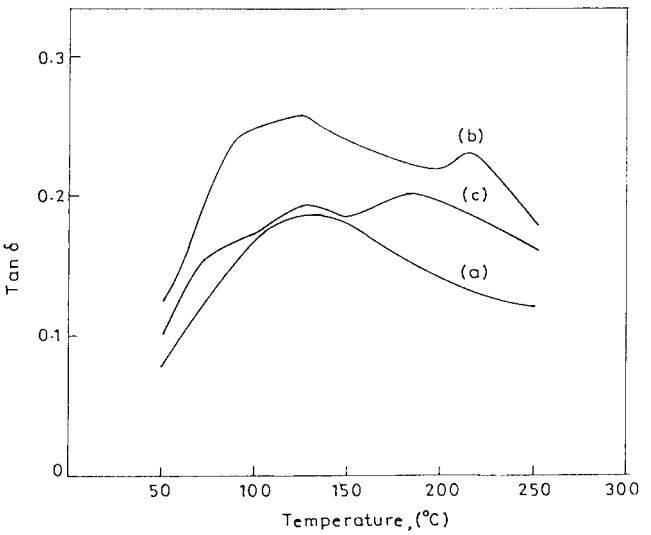

Figure 7 Variation in tan δ with temperature: (a) L_0 (100% EPDM), (b) L_1 (90/10 EPDM/LCP), and (c) L_2 (80/20 EPDM/LCP). The slab was made at 150°C with curative.

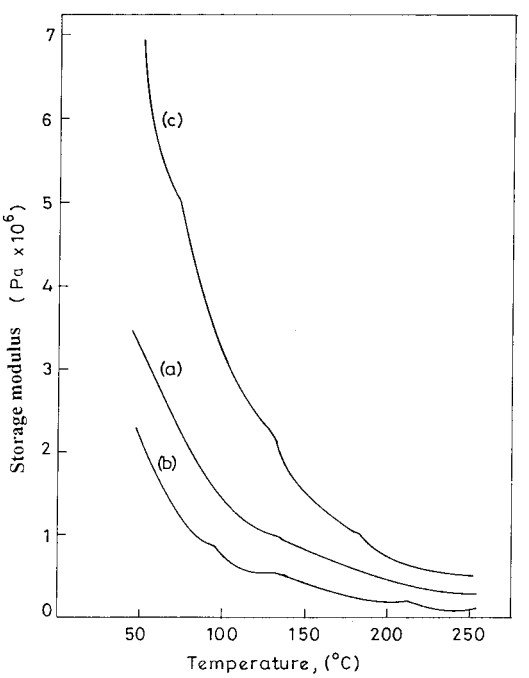

Figure 8 Variation in the dynamic modulus with temperature: (a) L_0 (100% EPDM), (b) L_1 (90/10 EPDM/LCP), and (c) L_2 (80/20 EPDM/LCP). The slab was made at 150°C with curative.

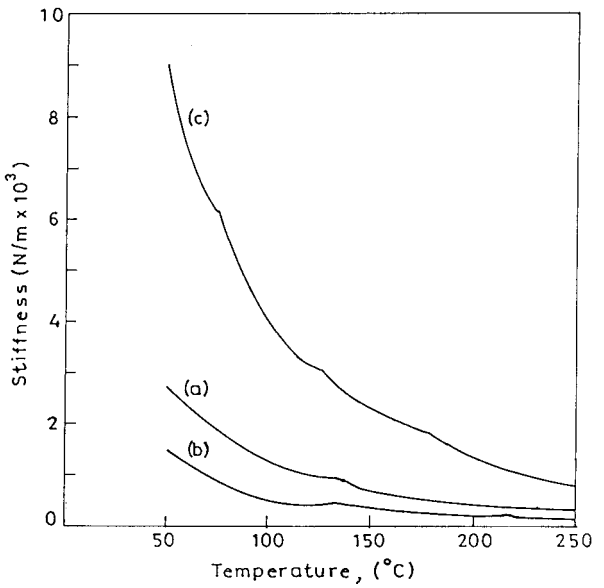

Figure 9 Variation in the stiffness with temperature: (a) L_0 (100% EPDM), (b) L_1 (90/10 EPDM/LCP), and (c) L_2 (80/20 EPDM/LCP). The slab was made at 150°C with curative.

peaks may have been the α' relaxation of the LCP. This type of relaxation generally occurs between the T_g and the melting temperature; hence, it could have been the α' relaxation of the LCP. With the initial addition of LCP in the blend (L_1), the loss peak values at all temperatures increased and then decreased at the 20% level of LCP (L_3). This increased loss values clearly indicated the contribution of micro-Brownian movement in the effective amorphous region for blend L_1, which was associated with increased crystallinity with increased P. With further increases in LCP (20%) in the L_2 blend, the loss peak values decreased, suggesting lower damping probably due to a lower molecular chain segment, which was free to move. For the L_1 blend, the higher damping was probably due to contribution from frozen-in segments, which could

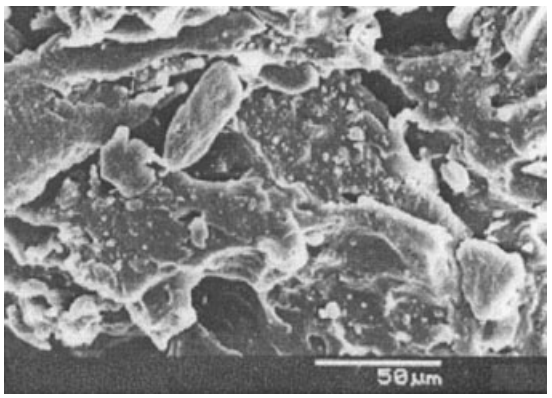

Figure 11 SEM photograph of the tensile fractured surface of the L_4 sample cured at 150°C.

store much more energy for a given deformation than free-to-move rubbery segments in the amorphous region. Thus, during every cycle of stress, the frozen-in segments became free to move, causing higher damping. The variations in the dynamic modulus and stiffness with temperature are shown in Figures 8 and 9. Both the parameters decreased with increasing temperature but at a different rate with three clear inflection points, depending on the blend ratio. 10% LCP probably gave rise to more or less uniform loss values over a wide range of temperature and may be the most suitable for dynamic applications.

SEM study

The phase morphology and the fracture mechanism, both under static and dynamic conditions, of the blends studied by SEM are represented in Figures 10–16. The tensile fracture sample of the pure EPDM (Fig. 10) showed a smooth rubbery failure. The crack originated from a point and had a diverging tendency associated with minimal void formation. In the presence of LCP and with subsequent curing with organic

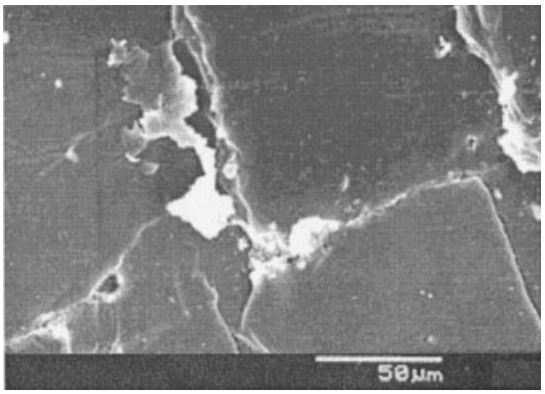

Figure 10 SEM photograph of the tensile fractured surface of the L_0 sample cured at 150°C.

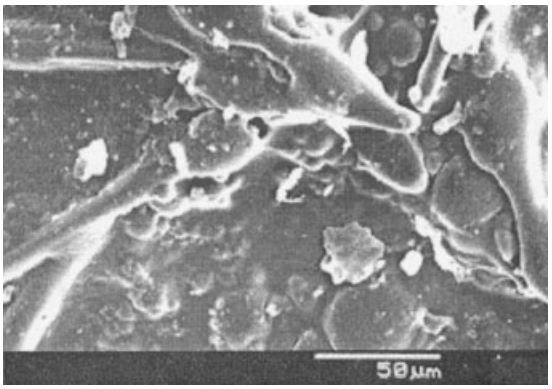

Figure 12 SEM photograph of the tensile fractured surface of sample L_4. The slab was made at 300°C without curative.

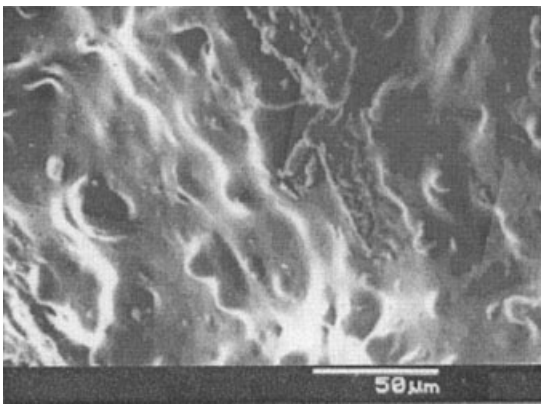

Figure 13 SEM photograph of the original L_4 sample.

peroxide at 150°C (Fig. 11), the fracture mechanism tended to change to a brittle one with increasing void formation. In this case, the fibrils were shortened because of further processing at lower temperature. The slabs made at 300°C without curative showed brittle failure with sufficient fibrillation accompanied by voids.

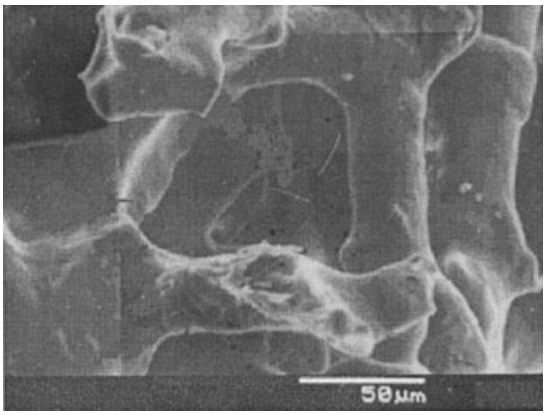

Figure 14 SEM photograph of the L_4 sample with THF extracted.

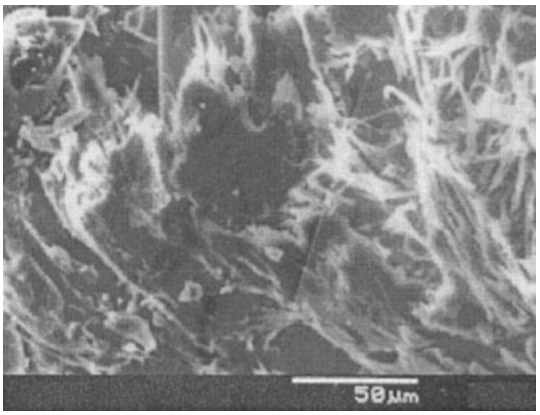

Figure 15 SEM photograph of the dynamic fractured surface of the L_4 sample cured at 150°C.

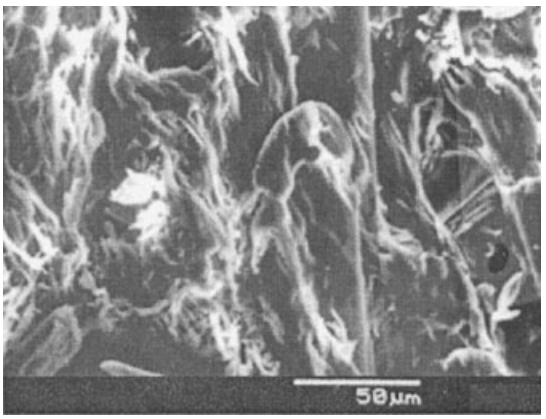

Figure 16 SEM photograph of the dynamic fractured surface of sample L_4. The slab was made at 300°C without curative.

The phase morphology of the blended sample (L_4) showed a smooth texture, suggesting a uniform distribution of the components and a better wettability of the fibrils by the matrix polymer (Fig. 13). The same sample when solvent-extracted (Fig. 14) showed an interconnecting structure of LCP fibrils.

The fractograms of the dynamically failed samples are shown in Figures 15 and 16. As is quite evident from the figures, fibrillation was prominent in both cases (Figs. 15 and 16) compared to the tensile fracture samples, perhaps due to high-temperature dynamic stress–strain cycles. The slab made at 300°C without curative (Fig. 16) showed a higher range fibrillation than the samples made at 150°C with curative (Fig. 15), where large-scale cavitation was evident.

CONCLUSIONS

EPDM and LCP blends seemed to be incompatible, although a better wetting of the LCP fibrils by the EPDM matrix was observed. Interconnecting fibrillation was possible under the shear field processing of the EPDM/LCP blends. Crystallinity seemed to be controlled by the processing temperature and the rate of cooling rather than crosslinking in the system. Fibrils became shorter with further processing of the blend at a lower temperature. LCP enhanced the thermal stability of the blend. Both frozen-in segments and effective amorphous zones probably controlled the dynamic properties of the EPDM/LCP composites.

References

1. Isayev, A. I.; Limtasiri, T. In International Encyclopedia of Composites; Lee, S. M., Ed.; VCH: New York, 1990; Vol. 3, p 55.
2. Kulichikhin, V. G.; Plate, N. A. Polym Sci USSR A 1991, 33, 3.
3. Dutta, D.; Fruitwala, H.; Kohli, A.; Weiss, R. A. Polym Eng Sci 1990, 30, 1005.

4. Handlos, A. A.; Baird, D. G. Marcromol Rev Chem Phys C 1995, 35, 183.
5. Vinogradov, G. V.; Malkin, A. Y. Rheology of Polymers; Mir: Moscow, 1980.
6. Min, K.; White, J. L.; Fellers, J. F. Polym Eng Sci 1984, 24, 1327.
7. Grace, H. P. Chem Eng Commun 1982, 14, 225.
8. Alle, N.; Lyngaae-Jorgensen, J. Rheol Acta 1980, 19, 104.
9. Karam, H.; Bellinger, G. L. Ind Eng Chem Fund 1968, 7, 576.
10. Han, C. D. Multiphase Flow; Academic: New York, 1981.
11. Vinogradov, G. V.; Yarlykov, B. V.; Tacbrenko, M. V.; Yudin, A. V.; Ablazova, T. I. Polymer 1975, 16, 609.
12. (a) Isayev, A. I.; Modic, M. Polym Compos 1987, 8, 158; (b) Isayev, A. I.; Modic, M. Soc Plast Eng Annu Tech Conf 1986, 32, 573.
13. (a) Blizard, K. G.; Baird, D. G. Polym Eng Sci 1987, 27, 653; (b) Blizard, K. G.; Baird, D. G. Soc Plast Eng Annu Tech Conf 1986, 32, 311.
14. Isayev, A. I.; Swaminathan, S. In Advanced Composites. III. Expanding Technology; American Society of Materials; 1987; p 259.
15. Mehta, A.; Isayev, A. I. Polym Eng Sci 1991, 31, 963.
16. Bassett, B. R.; Yee, A. F. Polym Compos 1990, 11, 10.
17. Hsu, T. C.; Lichkus, A. M.; Harrison, I. R. Polym Eng Sci 1993, 33, 860.
18. Dutta, D.; Weiss, R. A.; Kristal, K. Polym Eng Sci 1993, 33, 838.
19. Dutta, D.; Weiss, R. A.; Kristal, K. Polym Compos 1992, 13, 394.
20. Incarnato, L.; Nobile, M. R.; Frigione, M.; Motta, O.; Acierno, D. Int Polym Proc 1993, 8, 191.
21. Blizard, K. G.; Haghighat, R. R. Polym Eng Sci 1993, 33, 799.
22. Sharama, S. K.; Tendolkar, A.; Mishra, A. Mol Cryst Liq Cryst 1988, 157, 597.
23. Da Silva, L.; Bretas, R. E. S. Polym Eng Sci 2000, 40, 1414.
24. Turcott, E.; Nguyen, K. T.; Garcia-Rejon, A. Polym Eng Sci 2001, 41, 603.
25. Song, C. H.; Isayev, A. I. J Polym Eng 2000, 20, 427.
26. Qi, K.; Nakayama, K. J Mater Sci 2001, 36, 3207.
27. Pisharath, S. K.; Wong, S. C. Polym Eng Sci 2003, 24, 109.
28. Kim, B. C.; Hong, S. M. Mol Cryst Liq Cryst 1994, 254, 251.
29. Seo, Y.; Kim, K. U. Polym Eng Sci 1998, 38, 596.
30. Seo, Y.; Hwang, S. S.; Hong, S. M.; Park, T. S.; Kim, K. U. Polym Eng Sci 1995, 35, 1621.
31. Sahoo, N. G.; Das, C. K. Polym Plast Technol Eng 2002, 41, 619.
32. Verhoogt, H.; Langelaan, H. C.; Vandam, J.; De Boer, A. P. Polym Sci and Eng 1993, 33, 754.
33. Alexander, L. E. X-Ray Diffraction Methods in Polymer Science; Wiley Interscience: New York, 1969.
34. Roychowdhury, S.; Das, C. K. Polym Polym Compos 2000, 8, 177.
35. Martuscelli, E.; Riva, F.; Scllitti, C.; Silvestre, C. Polymer 1995, 26, 270.
36. Billingham, N. C. In Atmospheric Oxidation and Antioxidants, 2nd ed.; Elsevier Science: New York, 1993; Vol. II, Chapter 4.